

# Lawrence Berkeley National Laboratory

## LBL Publications

### Title

Full characterization of ultrathin 5-nm low-k dielectric bilayers: Influence of dopants and surfaces on the mechanical properties

### Permalink

<https://escholarship.org/uc/item/8zs5k49w>

### Journal

Physical Review Materials, 4(7)

### ISSN

2476-0455

### Authors

Frazer, Travis D  
Knobloch, Joshua L  
Hernández-Charpak, Jorge N  
[et al.](#)

### Publication Date

2020-07-01

### DOI

10.1103/physrevmaterials.4.073603

Peer reviewed

# Full characterization of ultrathin 5-nm low- $k$ dielectric bilayers: Influence of dopants and surfaces on the mechanical properties

Travis D. Frazer<sup>1,\*</sup>, Joshua L. Knobloch<sup>1</sup>, Jorge N. Hernández-Charpak<sup>1</sup>, Kathleen M. Hoogeboom-Pot<sup>1</sup>, Damiano Nardi<sup>1</sup>, Sadeq Yazdi<sup>2</sup>, Weilun Chao<sup>3</sup>, Erik H. Anderson<sup>3</sup>, Marie K. Tripp<sup>4</sup>, Sean W. King<sup>4</sup>, Henry C. Kapteyn<sup>1</sup>, Margaret M. Murnane<sup>1</sup> and Begoña Abad<sup>1</sup>

<sup>1</sup>*Department of Physics, JILA and STROBE NSF Science & Technology Center, University of Colorado and NIST, Boulder, Colorado 80309, USA*

<sup>2</sup>*Renewable and Sustainable Energy Institute, University of Colorado, Boulder, Colorado 80309, USA*

<sup>3</sup>*Center for X-Ray Optics, Lawrence Berkeley National Laboratory, Berkeley, California 94720, USA*

<sup>4</sup>*Intel Corp., 2501 NW 229th Ave., Hillsboro, Oregon 97124, USA*

Ultrathin films and multilayers, with controlled thickness down to single atomic layers, are critical for advanced technologies ranging from nanoelectronics to spintronics to quantum devices. However, for thicknesses less than 10 nm, surfaces and dopants contribute significantly to the film properties, which can differ dramatically from that of bulk materials. For amorphous films being developed as low dielectric constant interfaces for nanoelectronics, the presence of surfaces or dopants can soften films and degrade their mechanical performance. Here we use coherent short-wavelength light to fully and nondestructively characterize the mechanical properties of individual films as thin as 5 nm within a bilayer. In general, we find that the mechanical properties depend both on the amount of doping and the presence of surfaces. In very thin (5-nm) silicon carbide bilayers with low hydrogen doping, surface effects induce a substantial softening—by almost an order of magnitude—compared with the same doping in thicker (46-nm) bilayers. These findings are important for informed design of ultrathin films for a host of nano- and quantum technologies, and for improving the switching speed and efficiency of next-generation electronics.

## I. INTRODUCTION

Advanced nanoelectronics, spintronics, and quantum devices are becoming increasingly three dimensional in design, incorporating many layers of sub-10-nm ultrathin films. Moreover, these heterostructures must maintain optimal mechanical properties to avoid device failure. For example, softening due to high hydrogenation (doping with hydrogen) can lead to creep and delamination in semiconductor devices [1,2]. Additionally, as devices push to ever-smaller characteristic dimensions, the larger influence of surfaces and interfaces in nanoscale films can change the material properties compared to bulk materials. Depending on the composition of the film, nanoscale thickness effects have been shown to either soften or stiffen ultrathin films [3,4].

One mechanism for introducing a thickness dependence of the elastic properties of ultrathin films arises from the high proportion of atoms at the free surface of the material, which have a reduced number of nearest neighbors compared to atoms in the bulk volume. The low-coordinated surface can either soften the film since surface atoms have fewer constraints on their movement [5], or it can stiffen the film as redistributed electrons induce charging or bond contraction [6,7]. These mechanisms have been studied theoretically using continuum and atomistic approaches [5,7–11], and were

measured experimentally in materials such as nitrides [12], semiconductors [10,13], polymers [14], and metals [15–17]. A second mechanism that can modify the elastic properties of ultrathin films is the influence of interfaces in multilayers [18]. For example, in few-nanometer-thick Ni/Ta bilayers, while their density ratio is not meaningfully changed from that expected in bulk, we have previously shown their elastic properties are significantly modified—nickel softens while tantalum stiffens, relative to their bulk counterparts [4]. However, in this past work we could not extract both of the two elastic constants that fully describe isotropic materials, which are critical to understanding dielectrics for nanoelectronics.

Dielectric thin films such as SiC:H and SiOC:H promise optimal electrical properties that are critical for continued scaling of computing power, but struggle to maintain good mechanical properties. To improve the efficiency and switching speed of the final device, the dielectric constant,  $k$ , of the material between the metallic circuit elements (the interlayer dielectric) needs to be low, below that of the silica used historically ( $k = 4.2$ ) [1,19]. Methods to lower the dielectric constant include introducing more nonpolar bonds via hydrogenation, or introducing pores into the interlayer dielectric. However, the mechanical performance of the film degrades when the network of bonds in the bulk of the film becomes too disrupted, either by high levels of hydrogen bond termination [19–21] or porosity [22].

To measure the elastic properties of such thin films, it is very challenging for most techniques to probe <50-nm

\*travis.frazer@colorado.edu

79 thicknesses. Widely used techniques such as nanoindentation  
80 can characterize films with thicknesses on the order of a  
81 fraction of a micron, when combined with advanced modeling  
82 [23,24]. Surface Brillouin light scattering, which uses the  
83 interaction of light and acoustic phonons, has extracted the  
84 full elastic tensor of films of thicknesses down to 25 nm [25].  
85 However, it has difficulty characterizing thinner films without  
86 assuming one of the elastic constants. In past work, we used  
87 coherent extreme ultraviolet (EUV) beams to characterize the  
88 full elastic tensor of isotropic ultrathin films down to 11 nm  
89 in thickness [21]. This allowed us to simultaneously extract  
90 the Young modulus and Poisson’s ratio of low- $k$  amorphous  
91 SiC:H films with varying degrees of stiffness and hydrogenation,  
92 in a single measurement.

93 In this work, we show how dopants and surfaces inter-  
94 play to determine the elastic properties of low- $k$  ( $k < 4.2$ )  
95 dielectric films that are being developed for next-generation  
96 nanoelectronics. We use coherent short-wavelength light to  
97 fully and nondestructively characterize the mechanical prop-  
98 erties of SiOC:H films and SiC:H bilayers with individual  
99 layers as thin as 5 nm. This allows us to distinguish between  
100 dopant-induced and surface-induced softening. For example,  
101 in very thin (5-nm) silicon carbide films with low hydrogen  
102 doping, surface effects induce a substantial softening—by al-  
103 most an order of magnitude—compared with the same doping  
104 in thicker (46-nm) films. These findings are important for  
105 informed design of ultrathin films for a host of nano- and  
106 quantum technologies, and for improving the switching speed  
107 and efficiency of next-generation electronics.

## 108 II. METHODS

109 To distinguish between surface-induced softening and  
110 dopant-induced softening, we compare two different sample  
111 materials: high-hydrogenation amorphous SiC:H and low-  
112 hydrogenation amorphous SiOC:H. Each sample is fabricated  
113 by plasma-enhanced chemical vapor deposition from diluted  
114 organosilane precursors on 300-mm-diameter Si (001) by  
115 Intel Corp., as described in Refs. [19,26,27]. To describe  
116 the number of atomic bonds broken by hydrogenation in  
117 each material, we use nominal values of network connectivity  
118 (or average atomic coordination number), as determined by  
119 Rutherford backscattering and nuclear reaction analysis [28]  
120 at Intel Corp. See Supplemental Material for the nominal  
121 film properties, including  $k$  [29]. As described by topological  
122 constraint theory [30,31], an amorphous material transitions  
123 from flexible to rigid when the number of constraints on  
124 each atom,  $n$ , equals the number of degrees of freedom.  
125 Accounting for the fixed bond lengths and the fixed bond  
126 angles, the relation between network connectivity,  $\langle r \rangle$ , and  
127 constraints,  $n$ , is  $n = \langle r \rangle / 2 + (2\langle r \rangle - 3)$ . To constrain all  
128 three degrees of freedom,  $\langle r \rangle$  has a critical value at 2.4,  
129 known as the rigidity percolation threshold, where the co-  
130 ordination is high enough for a rigid network of bonds to  
131 percolate through the film volume. Our SiC:H samples have  
132  $\langle r \rangle = 3.2$ , and thus are rigid, while our SiOC:H samples have  
133 been hydrogenated to the critical value of 2.4, which makes  
134 films softer and less compressible, as we have previously  
135 shown [21]. By characterizing the elastic properties of several  
136 thicknesses of both materials, we investigate surface-induced

softening both above and below the critical level of hydrogen  
137 doping. 138

139 We characterize the elastic properties of ultrathin films  
140 using the EUV nanometrology technique described in  
141 Refs. [4,21,32]. First, we deposit an array of Ni nanoline  
142 grating transducers on each sample using e-beam lithography  
143 and liftoff. Grating periods range from 1.5  $\mu\text{m}$  to 40 nm,  
144 as characterized by atomic force microscopy [29,33]. We  
145 laser excite these transducers using an ultrafast (30-fs), near-  
146 infrared (780-nm) pump pulse, as illustrated in Fig. 1(a).  
147 The resulting impulsive thermal expansion of the nanolines  
148 launches acoustic waves in the nanolines and the film. At early  
149 times, a longitudinal acoustic wave propagates down into the  
150 sample and reflects from any buried interfaces back to the  
151 surface [Fig. 1(b)]. On longer timescales, a surface acoustic  
152 wave dominates, with a wavelength defined by the grating  
153 period [Fig. 1(c)]. The longitudinal breathing mode of the  
154 nanolines is also excited, which we have previously used to  
155 characterize the nanolines’ elastic properties [4] [Fig. 1(c)].

156 We measure these dynamic surface deformations by  
157 diffracting a time-delayed, ultrafast (10-fs) coherent EUV  
158 probe pulse from the surface. The probe has 29-nm wave-  
159 length (43-eV photon energy), obtained via high-harmonic  
160 generation [34]. This photon energy is far from any absorption  
161 edges in our sample materials, ensuring minimal sensitiv-  
162 ity to hot electrons, which can dominate visible-wavelength  
163 measurements at the few-picosecond timescales of interest  
164 to this work [e.g., Fig. 1(b)]. Our EUV probe provides a  
165 direct and sensitive ( $\sim\text{pm}$  sensitivity) [35] measurement of  
166 the surface acoustic waves and longitudinal acoustic waves  
167 in the film. By fitting the acoustic wave velocities using  
168 a finite-element analysis (FEA) procedure [21,36–38], we  
169 extract the two independent components of the isotropic elas-  
170 tic tensor of the film:  $c_{11}$  and  $c_{44}$ , or equivalently Young’s  
171 modulus and Poisson’s ratio (see Supplemental Material)  
172 [29,39].

## 173 III. RESULTS AND DISCUSSION

174 Our samples are deposited in two geometries: the SiC:H  
175 samples are bilayers (a stack of two identical layers on a  
176 Si substrate, see Fig. 2), and the SiOC:H samples are films  
177 (a single film on a Si substrate). The two SiC:H bilayer  
178 samples compare two different layer thicknesses, 46 and 5  
179 nm, and we extract the elastic properties of the topmost layer  
180 to check for softening due to the free surface. The SiOC:H  
181 films compare three different thicknesses, 44, 19, and 11  
182 nm, and have higher hydrogenation than the SiC:H bilayers,  
183 as already described. Most importantly, all of the samples  
184 we measure are nonporous. This isolates the influence of  
185 the single free surface at the top of the film stack. Porous  
186 SiOC:H has been shown to have constant elastic properties  
187 down to 25-nm thickness [22], but the pores create multiple  
188 surfaces throughout the volume of the film, complicating a  
189 comparison between surface-induced softening and doping-  
190 induced softening in that case.

191 To extract the mechanical properties of the ultrathin films,  
192 our model requires *a priori* thicknesses and densities for  
193 each film. X-ray reflectivity provides these values for the  
194 SiOC:H films [29], but it is unable to distinguish the individ-

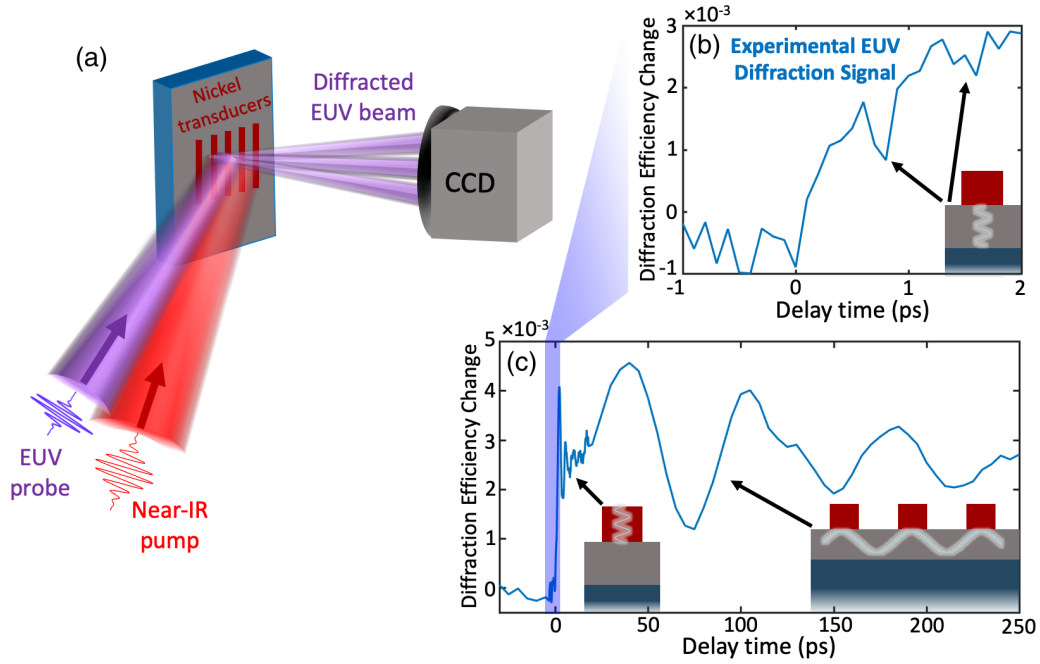


FIG. 1. Dynamic EUV diffraction from transverse and longitudinal acoustic waves. (a) After ultrafast laser excitation, the hot Ni nanolines impulsively expand, launching acoustic waves in the sample. After a controlled time delay, an EUV probe pulse diffracts from the sample surface, and the scattered light is collected by a charge-coupled device camera. The acoustic waves dynamically change the EUV diffraction efficiency, as shown in (b) and (c). (b) A longitudinal acoustic wave is launched downward into the film (inset). Reflections from the film-substrate interface imprint a discrete series of echoes in the data (see arrows in inset). (c) At early times, we observe the longitudinal breathing mode (left) of the nanolines. At longer times, we observe a surface acoustic wave (right), whose penetration depth is confined to a fraction of the grating period. The surface acoustic wave and longitudinal acoustic wave velocities provide the two independent components of the isotropic film's elastic tensor.

195 ual layer thicknesses in the SiC:H bilayers. For the bilayers,  
 196 we instead utilize scanning transmission electron microscopy  
 197 (STEM) and energy-dispersive x-ray spectroscopy (EDS)  
 198 to validate the precise thicknesses and compositions of all the  
 199 layers we expect in the bilayer samples, as shown in Fig. 2.  
 200 During sample fabrication, a nitrogen plasma treatment was  
 201 performed before each SiC:H layer deposition, creating two  
 202 additional 2-nm N-rich layers [Fig. 2(b)]. Moreover, as STEM  
 203 was performed after the EUV measurements, we also observe

204 a layer of amorphous carbon on top of the sample, which  
 205 both the electron and the EUV beams can deposit during the  
 206 measurement [40]. We also observe strain-induced contrast in  
 207 both the Si substrate and the lower SiC:H layer, which will be  
 208 discussed below.

209 To enhance the EUV measurement sensitivity to the influ-  
 210 ence of a free surface on the elastic properties of the film,  
 211 we confine the acoustic waves predominantly into the top  
 212 SiC:H layer. We do this by launching surface acoustic waves

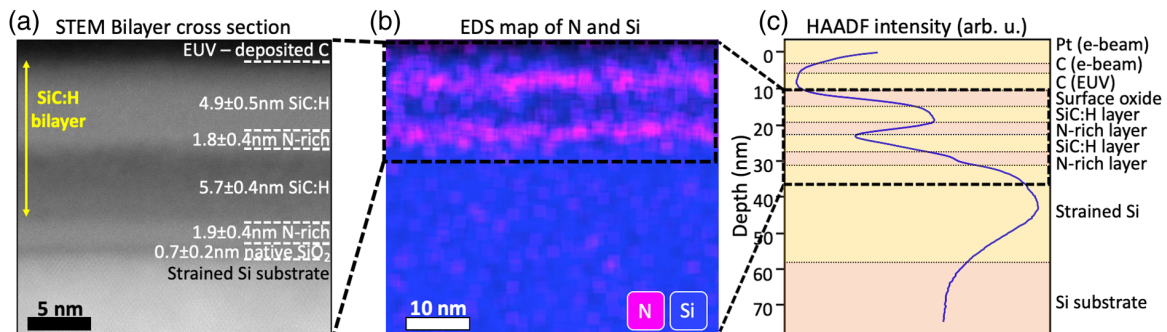


FIG. 2. Compositional characterization of the 5-nm SiC:H bilayer. (a) STEM image obtained using a HAADF detector. Strain from the deposited films blurs the atomic contrast peaks in the Si substrate, as expected [41]. HAADF intensity also drops at the interface of the two films in the bilayer. We attribute this to a reduction in the density of the bottom SiC:H layer, as it is strained by the layers above it. (b) EDS image of the sample showing Si (blue) and N (pink). Nitrogen exists at the bottom interfaces of the two SiC:H layers due to the nitrogen plasma clean applied to improve the film adhesion. (c) Horizontally binned lineout of the HAADF contrast for the full cross section taken for STEM characterization. This lineout extends upwards into the focused ion beam (FIB)-deposited Pt layer used for STEM, and downwards into the strained region of the Si substrate.

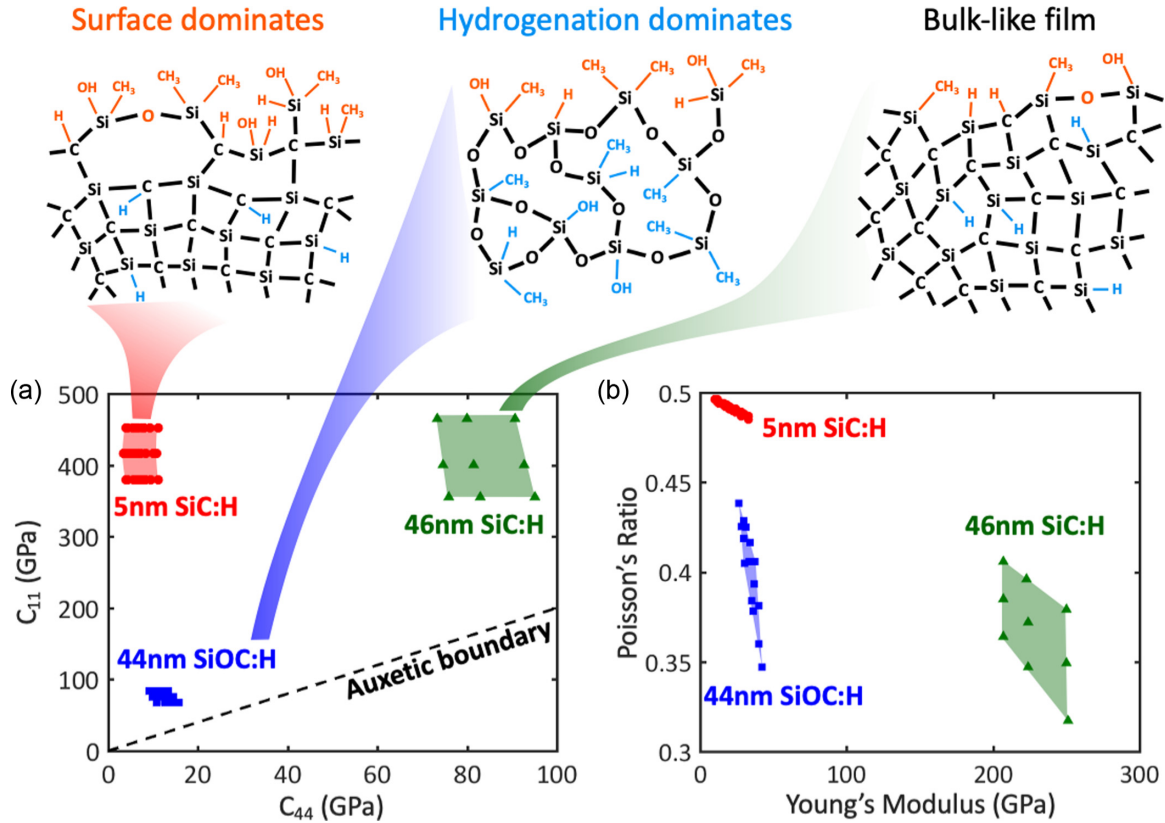


FIG. 3. Surface-induced softening compared to hydrogenation-induced softening. (a) Elastic constant ranges for the 5-nm SiC:H top layer (red circles), the 46-nm SiC:H top layer (green triangles), and the highly hydrogenated 44-nm SiOC:H film (blue squares). Each point represents a configuration simulated in the FEA model that agrees with the data, within uncertainty. The 46-nm film maintains a bulklike rigid bond network, due to its low hydrogenation and large thickness. The 5-nm film of the same material is significantly softened due to the terminated bonds at its surface (orange). This is distinct from the softening observed in highly hydrogenated SiOC:H, where hydrogenation breaks up the rigid bond network in the volume of the film (blue). Note the top schematics are to illustrate the differences between samples, and are not exact. The auxetic boundary, defined by  $c_{11} = 2c_{44}$ , is the limit where Poisson's ratio becomes negative. (b) The same data as in (a), expressed in terms of Poisson's ratio and Young's modulus.

with a 40-nm-period grating, which sets their wavelength and confines their penetration depth to  $\sim 1/\pi$  of this period [36,37,42]. With most of the elastic energy confined to the topmost layer, we are able to reliably fit the elastic properties without any contribution from spurious effects from the lower layers. We account for the effects of the EUV deposited carbon, N-rich layers, and strain in our FEA model, as described in the Supplemental Material [29,43–45].

As shown in Fig. 3, we observe a strong softening in the low-hydrogenation SiC:H top layer when the thickness is reduced from 46 to 5 nm. This is mainly due to a reduced value of  $c_{44}$ , while  $c_{11}$  stays approximately constant [Fig. 3(a)]. In terms of Young's modulus and Poisson's ratio [Fig. 3(b)], the 5-nm SiC:H layer has a lower Young's modulus but higher Poisson's ratio, i.e., it is softer and more incompressible, like a polymer film. Note that the range of allowed elastic properties defines a nonsquare region (shaded in Fig. 3), after propagating the symmetric experimental uncertainty through the analysis process (see Supplemental Material [29]). While the 46-nm top layer maintains a bulklike rigid bond network, due to its low hydrogenation and large thickness, the 5-nm top layer of the same material is significantly softened due to the terminated bonds at its surface (orange in Fig. 3). This

behavior is distinct from the softening observed in highly hydrogenated SiOC:H, where hydrogenation breaks up the rigid bond network in the volume of the film (blue in Fig. 3). This measurement of the 5-nm SiC:H layer represents the full characterization of a  $< 10$  nm film without assuming any of the elastic constants.

The results on high-hydrogenation SiOC:H contrast with the results on low-hydrogenation SiC:H. First, the SiOC:H films have been hydrogenated past the critical number of broken bonds, meaning that the thickest, 44-nm film is expected to have lower  $c_{11}$  and  $c_{44}$  values than the SiC:H samples [Fig. 3(a)]. This places the region of allowed elastic constants close to the auxetic boundary, defined by  $c_{11} = 2c_{44}$ , below which Poisson's ratio becomes negative. This appears as a larger distortion after converting to Young's modulus and Poisson's ratio [Fig. 3(b)]. Comparing different SiOC:H film thicknesses, there is no discernible change in elastic properties since the regions of allowed elastic properties overlap for all three film thicknesses, with the only difference being an increased experimental uncertainty for the thinner films. For clarity, only the thickest SiOC:H film is shown in Fig. 3, but all three films' results are shown in the Supplemental Material [29].

236  
237  
238  
239  
240  
241  
242  
243  
244  
245  
246  
247  
248  
249  
250  
251  
252  
253  
254  
255  
256  
257  
258

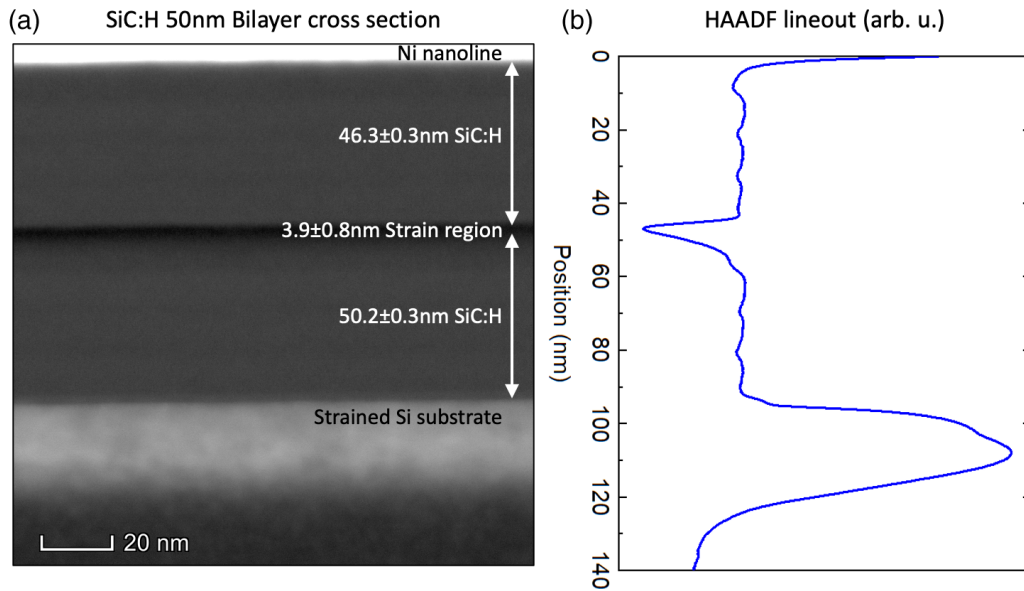


FIG. 4. STEM cross section of 46-nm SiC:H bilayer. (a) Full HAADF image. SiC:H films are known to strain Si substrates, and the full depth of the strained volume is visible here in the blurring of the atomic peaks imaged in the substrate region. We attribute the low-intensity region between the two SiC:H layers to a reduction in density as the top layer and N-rich layer similarly strain the bottom layer. Note the thickness of this strained region is similar to the layer thickness for the 5-nm bilayer in Fig. 2(a), indicating the same effect is lowering the HAADF intensity in the bottom layer of both SiC:H samples. (b) Lineout by horizontally binning (a). The faint intensity striations within each SiC:H layer are a result of the four-step deposition process. Each step is identical, with no change in film composition.

259 From the results presented above, we observe no surface-  
 260 induced softening in highly hydrogenated SiOC:H, but we observe  
 261 a significant surface-induced softening in lowly hydrogenated  
 262 SiC:H. Our measurements indicate that this behavior comes from a competition between bond termination at the  
 263 free surface, and bond termination in the bulk of the film due  
 264 to hydrogenation. Both of these mechanisms reduce the rigid  
 265 constraints on atoms, but only so many bonds can be terminated  
 266 before a critical threshold is passed and the material loses its rigidity. As described above, the SiOC:H films have  
 267 surpassed this critical threshold due to hydrogenation alone.  
 268 Thus, the free surface can only have a minimal effect as the  
 269 film thickness is reduced. The SiC:H bilayers, however, have  
 270 less hydrogenation, well below the critical threshold. This  
 271 allows the top layer to have a greater difference between the  
 272 rigid bond network in its volume, and the terminated bonds at  
 273 its free surface. When the layer thickness is reduced, the free  
 274 surface can then begin to dominate over the otherwise rigid  
 275 volume of SiC:H, softening the entire top layer. Importantly,  
 276 the softening we observe in the 5-nm bilayer is not due to  
 277 oxidation making the SiC:H equivalent to the SiOC:H films.  
 278 X-ray photoelectron spectroscopy has shown SiC:H to be  
 279 highly oxidation resistant [46,47], so any oxygen content in  
 280 the SiC:H bilayer is much lower than in the SiOC:H films and  
 281 likely is confined only to the outermost atomic layer, as indicated  
 282 in Fig. 3 and corroborated by EDS (see Supplemental Material) [29].  
 283 Moreover, oxygen is twofold coordinated, so its presence still has  
 284 the net effect of reducing the surface bond coordination.  
 285

286 To confirm the interpretation of our results as a surface  
 287 softening effect, we perform further STEM and EDS characterizations  
 288 of the thicker SiC:H bilayer to verify that it is identical in  
 289 composition to the thinner bilayer. In the STEM cross  
 290 section of the 46-nm bilayer (see Fig. 4), we observe similar  
 291 changes in layer contrast as in the 5-nm bilayer. Specifically,  
 292 we observe a region of reduced high-angle annular dark-field  
 293 (HAADF) intensity at the top of the lower layer (just below  
 294 the N-rich layer). Because the SiC:H layers are thicker for  
 295 this sample, we can see here that the reduced intensity has a  
 296 finite penetration depth of about 4 nm into the lower layer.  
 297 This depth is comparable to the layer thickness of the thinner  
 298 bilayer sample, and so we attribute the intensity reduction in  
 299 both samples to the top layer straining the bottom layer. We  
 300 similarly observe a clear strain layer in the Si substrate due to  
 301 the lower SiC:H layer, as expected for such films on Si [41].  
 302 For the EDS measurements, there is no direct sensitivity to  
 303 hydrogen, but they provide a self-consistent evaluation of the  
 304 relative amounts of Si, C, O, and N through the depth of each  
 305 bilayer sample. For both the top and bottom SiC:H layers of  
 306 both the 5- and 46-nm bilayers, we measure consistent values  
 307 of  $\sim 85\%$  Si,  $\sim 12\%$  C, and  $<2\%$  each of O and N, which  
 308 is within the noise floor. See the Supplemental Material for  
 309 full EDS maps of each bilayer [29]. These characterizations  
 310 together confirm there is no large discrepancy in fabrication  
 311 between the two bilayer samples, and the primary difference  
 312 between them is layer thickness.  
 313 Finally, we rule out alternative explanations for the change  
 314 in elastic properties between the two SiC:H bilayers. First,  
 315 a large strain reducing the density of the lower layer cannot  
 316 explain our results. Reduced density would systematically  
 317 shift our results toward higher elastic constants (an opposite  
 318 trend to our observations)—moreover, our fitting procedure is  
 319 largely insensitive to the density of the lower layer. Second,  
 320 our observations cannot be explained by the nitrogen plasma  
 321 treatment. If the treatment was causing a change in the elastic  
 322 properties of lower layers, then the effect should be even more  
 323

292 section of the 46-nm bilayer (see Fig. 4), we observe similar  
 293 changes in layer contrast as in the 5-nm bilayer. Specifically,  
 294 we observe a region of reduced high-angle annular dark-field  
 295 (HAADF) intensity at the top of the lower layer (just below  
 296 the N-rich layer). Because the SiC:H layers are thicker for  
 297 this sample, we can see here that the reduced intensity has a  
 298 finite penetration depth of about 4 nm into the lower layer.  
 299 This depth is comparable to the layer thickness of the thinner  
 300 bilayer sample, and so we attribute the intensity reduction in  
 301 both samples to the top layer straining the bottom layer. We  
 302 similarly observe a clear strain layer in the Si substrate due to  
 303 the lower SiC:H layer, as expected for such films on Si [41].  
 304 For the EDS measurements, there is no direct sensitivity to  
 305 hydrogen, but they provide a self-consistent evaluation of the  
 306 relative amounts of Si, C, O, and N through the depth of each  
 307 bilayer sample. For both the top and bottom SiC:H layers of  
 308 both the 5- and 46-nm bilayers, we measure consistent values  
 309 of  $\sim 85\%$  Si,  $\sim 12\%$  C, and  $<2\%$  each of O and N, which  
 310 is within the noise floor. See the Supplemental Material for  
 311 full EDS maps of each bilayer [29]. These characterizations  
 312 together confirm there is no large discrepancy in fabrication  
 313 between the two bilayer samples, and the primary difference  
 314 between them is layer thickness.  
 315 Finally, we rule out alternative explanations for the change  
 316 in elastic properties between the two SiC:H bilayers. First,  
 317 a large strain reducing the density of the lower layer cannot  
 318 explain our results. Reduced density would systematically  
 319 shift our results toward higher elastic constants (an opposite  
 320 trend to our observations)—moreover, our fitting procedure is  
 321 largely insensitive to the density of the lower layer. Second,  
 322 our observations cannot be explained by the nitrogen plasma  
 323 treatment. If the treatment was causing a change in the elastic  
 324 properties of lower layers, then the effect should be even more

324

325 pronounced when studying a multilayer SiC:H stack with a  
326 plasma treatment on each layer. In Ref. [26], the authors  
327 perform nanoindentation on exactly this case, with identical  
328 SiC:H layers as in our samples. They observe no significant  
329 difference in the average elastic properties of the multilayers,  
330 both with and without the plasma treatment, down to a layer  
331 thickness of 2.6 nm. This indicates buried N-rich layers do  
332 not change the overall elastic properties of a stack of SiC:H  
333 films. Our technique, however, enables us to isolate only  
334 the top layer of our bilayer samples, where the free surface  
335 dominates, independent of any plasma treatment on the lower  
336 layer. Lastly, we cannot fit our data with nominal SiC:H  
337 layer properties while only varying the elastic constants of the  
338 N-rich interface layers.

#### 339 IV. CONCLUSION

340 We use coherent EUV beams to fully characterize the  
341 mechanical properties of films as thin as 5 nm. We find that in  
342 the top 5-nm layer of a SiC:H bilayer, surface effects induce  
343 a substantial softening—by almost an order of magnitude—  
344 compared with thicker, 46-nm SiC:H bilayers. This contrasts  
345 with SiOC:H films at high hydrogenation levels, which have  
346 no significant surface-induced softening, down to 11 nm. We

347 attribute this difference between the two sample sets to the  
348 competing effects of terminated bonds in the volume of the  
349 film due to hydrogenation, and the terminated bonds defining  
350 the free surface of the film. For the free surface to change film  
351 elastic properties, the surface atoms must be undercoordinated  
352 compared to the atoms in the volume of the film. Once hy-  
353 drogenation terminates enough bonds in the bulk of the film,  
354 atoms in the volume and surface of the film no longer have  
355 significantly different coordination numbers, and no thickness  
356 dependence is observed. These findings are important for  
357 informed design of ultrathin, robust films for a host of nano-  
358 and quantum technologies, and particularly for improving the  
359 switching speed and efficiency of next-generation electronics.

#### 360 ACKNOWLEDGMENTS

361 The authors gratefully acknowledge support from the  
362 STROBE National Science Foundation Science & Technol-  
363 ogy Center, Grant No. DMR-1548924 and a Gordon and  
364 Betty Moore Foundation EPiQS Award through Grant No.  
365 GBMF4538. J.L.K. acknowledges support from an SRC Fel-  
366 lowship. H.C.K. is partially employed by KMLabs. W.C.  
367 gratefully acknowledges support through the US Department  
368 of Energy under Contract No. DE-AC02-05CH11231.

- [1] D. Shamiryany, T. Abell, F. Iacopi, and K. Maex, Low-k dielectric materials, *Mater. Today* **7**, 34 (2004).
- [2] A. Grill, S. M. Gates, T. E. Ryan, S. V. Nguyen, and D. Priyadarshini, Progress in the development and understanding of advanced low k and ultralow k dielectrics for very large-scale integrated interconnects—state of the art, *Appl. Phys. Rev.* **1**, 011306 (2014).
- [3] L. G. Zhou and H. Huang, Are surfaces elastically softer or stiffer? *Appl. Phys. Lett.* **84**, 1940 (2004).
- [4] K. M. Hoogeboom-Pot, E. Turgut, J. N. Hernandez-Charpak, J. M. Shaw, H. C. Kapteyn, M. M. Murnane, and D. Nardi, Nondestructive measurement of the evolution of layer-specific mechanical properties in sub-10 nm bilayer films, *Nano Lett.* **16**, 4773 (2016).
- [5] R. J. Wang, C. Y. Wang, and Y. T. Feng, Effective geometric size and bond-loss effect in nanoelasticity of GaN nanowires, *Int. J. Mech. Sci.* **130**, 267 (2017).
- [6] C. Q. Sun, Size dependence of nanostructures: Impact of bond order deficiency, *Prog. Solid State Chem.* **35**, 1 (2007).
- [7] C. A. Yuan, O. van der Sluis, G. Q. Zhang, L. J. Ernst, W. D. van Driel, R. B. R. van Silfhout, and B. J. Thijssse, Chemical-mechanical relationship of amorphous/porous low-dielectric film materials. *Comput. Mater. Sci.* **42**, 606 (2008).
- [8] R. E. Miller and V. B. Shenoy, Size-dependent elastic properties of nanosized structural elements, *Nanotechnology* **11**, 139 (2000).
- [9] R. Dingreville, J. Qu, and M. Cherkaoui, Surface free energy and its effect on the elastic behavior of nano-sized particles, wires and films, *J. Mech. Phys. Solids* **53**, 1827 (2005).
- [10] A. I. Fedorchenko, A.-B. Wang, and H. H. Cheng, Thickness dependence of nanofilm elastic modulus, *Appl. Phys. Lett.* **94**, 152111 (2009).
- [11] B. Gong, Q. Chen, and D. Wang, Molecular dynamics study on size-dependent elastic properties of silicon nanoplates. *Mater. Lett.* **67**, 165 (2012).
- [12] D. C. Hurley, V. K. Tewary, and A. J. Richards, Thin-film elastic-property measurements with laser-ultrasonic SAW spectrometry, *Thin Solid Films* **398–399**, 326 (2001).
- [13] X. Li, T. Ono, Y. Wang, and M. Esashi, Ultrathin single-crystalline-silicon cantilever resonators: Fabrication technology and significant specimen size effect on young’s modulus, *Appl. Phys. Lett.* **83**, 3081 (2003).
- [14] C. M. Stafford, B. D. Vogt, C. Harrison, D. Julthongpipit, and R. Huang, Elastic moduli of ultrathin amorphous polymer films, *Macromolecules* **39**, 5095 (2006).
- [15] P.-O. Renault, E. Le Bourhis, P. Villain, Ph. Goudeau, K. F. Badawi, and D. Faurie, Measurement of the elastic constants of textured anisotropic thin films from x-ray diffraction data, *Appl. Phys. Lett.* **83**, 473 (2003).
- [16] H. Ogi, M. Fujii, N. Nakamura, T. Shagawa, and M. Hirao, Resonance acoustic-phonon spectroscopy for studying elasticity of ultrathin films, *Appl. Phys. Lett.* **90**, 191906 (2007).
- [17] H. Ogi, M. Fujii, N. Nakamura, T. Yasui, and M. Hirao, Stiffened Ultrathin Pt Films Confirmed by Acoustic-Phonon Resonances, *Phys. Rev. Lett.* **98**, 195503 (2007).
- [18] N. Nakamura, H. Ogi, T. Yasui, M. Fujii, and M. Hirao, Mechanism of Elastic Softening Behavior in a Superlattice, *Phys. Rev. Lett.* **99**, 035502 (2007).
- [19] S. W. King, J. Bielefeld, G. Xu, W. A. Lanford, Y. Matsuda, R. H. Dauskardt, N. Kim, D. Hondongwa, L. Olasov, B. Daly, G. Stan, M. Liu, D. Dutta, and D. Gidley, Influence of network bond percolation on the thermal, mechanical, electrical and optical properties of high and low-k a-SiC:H thin films, *J. Non-Cryst. Solids* **379**, 67 (2013).

- [20] H. Li, J. M. Knaup, E. Kaxiras, and J. J. Vlassak, Stiffening of organosilicate glasses by organic cross-linking, *Acta Mater.* **59**, 44 (2011).
- [21] J. N. Hernandez-Charpak, K. M. Hoogeboom-Pot, Q. Li, T. D. Frazer, J. L. Knobloch, M. Tripp, S. W. King, E. H. Anderson, W. Chao, M. M. Murnane, H. C. Kapteyn, and D. Nardi, Full characterization of the mechanical properties of 11–50 Nm ultrathin films: Influence of network connectivity on the poisson's ratio, *Nano Lett.* **17**, 2178 (2017).
- [22] J. Zizka, S. King, A. Every, and R. Sooryakumar, Acoustic phonons and mechanical properties of ultra-thin porous low-k films: A surface brillouin scattering study, *J. Electron. Mater.* **47**, 3942 (2018).
- [23] K. Geng, F. Yang, and E. A. Grulke, Nanoindentation of sub-micron polymeric coating systems, *Mater. Sci. Eng. A* **479**, 157 (2008).
- [24] J. Hay and B. Crawford, Measuring substrate-independent modulus of thin films, *J. Mater. Res.* **26**, 727 (2011).
- [25] J. Zizka, S. King, A. G. Every, and R. Sooryakumar, Mechanical properties of low- and high-k dielectric thin films: A surface brillouin light scattering study. *J. Appl. Phys.* **119**, 144102 (2016).
- [26] A. Giri, S. W. King, W. A. Lanford, A. B. Mei, D. Merrill, L. Li, R. Oviedo, J. Richards, D. H. Olson, J. L. Braun, J. T. Gaskins, F. Deangelis, A. Henry, and P. E. Hopkins, Interfacial defect vibrations enhance thermal transport in amorphous multilayers with ultrahigh thermal boundary conductance. *Adv. Mater.* **30**, 1804097 (2018).
- [27] S. W. King, M. M. Paquette, J. W. Otto, A. N. Caruso, J. Brockman, J. Bielefeld, M. French, M. Kuhn, and B. French, Valence and conduction band offsets at amorphous hexagonal boron nitride interfaces with silicon network dielectrics, *Appl. Phys. Lett.* **104**, 102901 (2014).
- [28] W. A. Lanford, M. Parenti, B. J. Nordell, M. M. Paquette, A. N. Caruso, M. Mäntymäki, J. Hämäläinen, M. Ritala, K. B. Klepper, V. Miikkulainen, O. Nilsen, W. Tenhaeff, N. Dudley, D. Koh, S. K. Banerjee, E. Mays, J. Bielefeld, and S. W. King, Nuclear reaction analysis for H, Li, Be, B, C, N, O and F with an RBS check, *Nucl. Instrum. Methods Phys. Res. B* **371**, 211 (2016).
- [29] See Supplemental Material at <http://link.aps.org/supplemental/10.1103/PhysRevMaterials.xx.xxxxxx> for tables of sample properties, measurement and analysis details, additional TEM images, and the full elastic properties results on SiOC:H films.
- [30] J. C. Phillips and M. F. Thorpe, Constraint theory, vector percolation and glass formation, *Solid State Commun.* **53**, 699 (1985).
- [31] J. C. Mauro, Topological constraint theory of glass, *Am. Ceram. Soc. Bull.* **90**, 31 (2011).
- [32] Q. Li, K. Hoogeboom-Pot, D. Nardi, M. M. Murnane, H. C. Kapteyn, M. E. Siemens, E. H. Anderson, O. Hellwig, E. Dobisz, B. Gurney, R. Yang, and K. A. Nelson, Generation and control of ultrashort-wavelength two-dimensional surface acoustic waves at nanoscale interfaces, *Phys. Rev. B* **85**, 195431 (2012).
- [33] I. Horcas, R. Fernández, J. M. Gómez-Rodríguez, J. Colchero, J. Gómez-Herrero, and A. M. Baro, WSXM: A software for scanning probe microscopy and a tool for nanotechnology, *Rev. Sci. Instrum.* **78**, 013705 (2007).
- [34] A. Rundquist, C. G. Durfee, Z. Chang, C. Herne, S. Backus, M. M. Murnane, and H. C. Kapteyn, Phase-matched generation of coherent soft X-rays, *Science* **280**, 1412 (1998).
- [35] R. I. Tobey, M. E. Siemens, O. Cohen, M. M. Murnane, H. C. Kapteyn, and K. A. Nelson, Ultrafast extreme ultraviolet holography: Dynamic monitoring of surface deformation, *Opt. Lett.* **32**, 286 (2007).
- [36] D. Nardi, F. Banfi, C. Giannetti, B. Revaz, G. Ferrini, and F. Parmigiani, Pseudosurface acoustic waves in hypersonic surface phononic crystals, *Phys. Rev. B* **80**, 104119 (2009).
- [37] D. Nardi, M. Travaglini, M. E. Siemens, Q. Li, M. M. Murnane, H. C. Kapteyn, G. Ferrini, F. Parmigiani, and F. Banfi, Probing thermomechanics at the nanoscale: Impulsively excited pseudo-surface acoustic waves in hypersonic phononic crystals. *Nano Lett.* **11**, 4126 (2011).
- [38] COMSOL, Inc., COMSOL Multiphysics, Version 4.3b (COMSOL, Inc., 2013).
- [39] L. Bluestein, A Linear Filtering Approach to the Computation of Discrete Fourier Transform, *IEEE Trans. Audio Electroacoust.* **18**, 451 (1970).
- [40] J. Chen, E. Louis, C. J. Lee, H. Wormeester, R. Kunze, H. Schmidt, D. Schneider, R. Moors, W. Schaik, M. Lubomska, and F. Bijkerk, Detection and Characterization of Carbon Contamination on EUV Multilayer Mirrors, *Opt. Express* **17**, 16969 (2009).
- [41] T. Denneulin, D. Cooper, J.-M. Hartmann, and J.-L. Rouviere, The addition of strain in uniaxially strained transistors by both SiN contact etch stop layers and recessed SiGe sources and drains, *J. Appl. Phys.* **112**, 094314 (2012).
- [42] B. Abad Mayor, J. L. Knobloch, T. D. Frazer, J. N. Hernandez-Charpak, H. Y. Cheng, A. J. Grede, N. C. Giebink, T. E. Mallouk, P. Mahale, N. N. Nova, A. A. Tomaschke, V. L. Ferguson, V. H. Crespi, V. Gopalan, H. C. Kapteyn, J. V. Badding, and M. M. Murnane, Nondestructive measurements of the mechanical and structural properties of nanostructured metalattices, *Nano Lett.* **20**, 3306 (2020).
- [43] J. L. Arlein, S. E. M. Palaich, B. C. Daly, P. Subramonium, and G. A. Antonelli, Optical pump-probe measurements of sound velocity and thermal conductivity of hydrogenated amorphous carbon films, *J. Appl. Phys.* **104**, 033508 (2008).
- [44] H. T. Grahm, H. J. Maris, J. Tauc, and B. Abeles, Time-resolved study of vibrations of a-Ge:H/a-Si:H multilayers, *Phys. Rev. B* **38**, 6066 (1988).
- [45] C. Rossignol, B. Perrin, B. Bonello, P. Djemia, P. Moch, and H. Hurdequint, Elastic properties of ultrathin permalloy/alumina multilayer films using picosecond ultrasonics and brillouin light scattering, *Phys. Rev. B* **70**, 094102 (2004).
- [46] Y. Matsuda, S. W. King, J. Bielefeld, J. Xu, and R. H. Dauskardt, Fracture properties of hydrogenated amorphous silicon carbide thin films, *Acta Mater.* **60**, 682 (2012).
- [47] Y. Matsuda, S. W. King, and R. H. Dauskardt, Tailored amorphous silicon carbide barrier dielectrics by nitrogen and oxygen doping, *Thin Solid Films* **531**, 552 (2013).